1   # Links between soil moisture and InSAR data on a temperate raised

2   # peatland subjected to a wildfire

3   Alexis Hrysiewicz[1,2,*], Eoghan P. Holohan[1,2], Shane Donohue[1,3] and Hugh Cushnan[4]

4   [1]Irish Centre for Research in Applied Geosciences (iCRAG), University College Dublin, Belfield,

5   Dublin 4, Ireland

6   [2] UCD School of Earth Sciences, University College Dublin, Belflied, Dublin 4, Ireland

7   [3] UCD School of Civil Engineering, University College Dublin, Belflied, Dublin 4, Ireland

8   [4] RPS Group, Elmwood House, 74 Boucher Road, Belfast, BT12 6RZ Northern Ireland, United

9   Kingdom

10   **Corresponding author: Alexis Hrysiewicz (alexis.hrysiewicz@ucd.ie)**

Earth ArXiv

15
16

Links between soil moisture and InSAR data on a temperate raised peatland subjected to a wildfire

Alexis Hrysiewicz[1,2,*], Eoghan P. Holohan[1,2], Shane Donohue[1,3] and Hugh Cushnan[4]

[1]Irish Centre for Research in Applied Geosciences (iCRAG), University College Dublin, Belfield, Dublin 4, Ireland

[2] UCD School of Earth Sciences, University College Dublin, Belflied, Dublin 4, Ireland

[3] UCD School of Civil Engineering, University College Dublin, Belflied, Dublin 4, Ireland

[4] RPS Group, Elmwood House, 74 Boucher Road, Belfast, BT12 6RZ Northern Ireland, United Kingdom

Corresponding author: Alexis Hrysiewicz (alexis.hrysiewicz@ucd.ie)

Highlights

- InSAR time-series analysis for measurement of ground motion on a raised peatland.

- InSAR is critically influenced by soil moisture changes and temporal baselines.

- Short-term coherence (< 1 year) is mainly controlled by soil moisture changes.

- A wildfire on the raised peatland caused little perturbance of InSAR measurements.

- Backscatter intensity and InSAR phase represent different parts of the peat column.

Abstract

Interferometry of Synthetic Aperture Radar (InSAR) can potentially contribute to the cost-effective regional or global monitoring of the degradation and restoration of peatlands. However, there are uncertainties about the links between InSAR results and peatland ecohydrological parameters, especially soil moisture. Here, we analyse the relationships between the temporal evolutions of InSAR coherence, ground displacements, and in-situ soil moisture measurements for a temperate raised bog at Ballynafagh, Co. Kildare, Ireland, in the period 2017-mid-2021. We also investigate the effects of a wildfire in June-July 2019 on those relationships. InSAR-derived ground displacements from Sentinel-1 C-band radar data indicate long-term subsidence of the intact and Active Raised Bog. Superimposed on the long-term displacement trends are annual oscillations that are linked to variations in rainfall and temperature and that are in phase with changes in soil moisture. We show that InSAR coherence is directly related to the change in soil moisture, with large changes causing coherence decrease or loss. The wildfire removed a 10-20 cm thick mossy vegetation layer across 60-70 % of the intact bog area. The radar backscatter intensity increased after the wildfire, but the InSAR coherence, the InSAR-derived surface displacements and the soil moisture were not noticeably affected. We therefore infer that C-band radar waves attenuate in the active vegetation layer, but penetrate through it into the upper few 10's of cm of the underlying peat. The radar backscatter occurs primarily at this level in the peat, where its coherence is controlled by the soil moisture. These findings underpin application and interpretation of radar for monitoring of peatlands, even if affected by wildfires, which are forecast to increase in both frequency and intensity due to global warming.

53 1. Introduction

54 Peatlands are one of the largest carbon sinks on Earth: an estimated 20-30 % of global soil carbon is

55 to be stored in peat, despite fens and bogs covering only a small percentage of the world's land surface

56 (Drösler et al., 2008; Gorham, 1991; Köchy et al., 2015; Renou-Wilson et al., 2019; Yu et al., 2010).

57 However, the role of peatlands in greenhouse-gas (GHG) emissions on global emissions is still

58 unknown or poorly quantified, and so closing this knowledge gap has been become a priority in the

59 context of mitigating global warming (Hiraishi et al., 2014; Leifeld & Menichetti, 2018; Roulet,

60 2000). In addition, peatland restoration is a focus of current mitigation efforts, (Renou-Wilson et al.,

61 2019), both to maintain the capacity of peatland to be GHG sinks, and also to preserve their endemic

62 flora and fauna, (Parish et al., 2008). Peatlands have been monitored traditionally through in-situ

63 measurements of various key ecohydrological parameters, (e.g., ground level, soil moisture,

64 temperature, groundwater levels, water balance, etc.) and GHG emissions. However, our ability to

65 extend such monitoring of peatlands to regional, national or global scales is a challenge. In Ireland,

66 for example, approximately 15 % of the island – c. 12,700 out of 84,400 km^2 - is covered by peat

67 soils (Connolly & Holden, 2009). Globally, 2.84 % of the world land area, amounting to 4.23 million

68 km^2, is peatland (Xu et al., 2018).

69 Spatial remote sensing has complemented in-situ measurements, providing quantification of

70 peatlands over large areas for several years, (e.g., Connolly & Holden, 2009; Connolly et al., 2007;

71 Jones et al., 2009). Satellite data allow estimates of many ecohydrological parameters to be

72 processed, with worldwide coverage, high accuracy and low cost (data being increasingly open-

73 source and free of charge to end-user), (Lees et al., 2018). For example, methods using the backscatter

74 intensity of synthetic aperture radar (SAR) have been developed to estimate soil moisture at medium

75   spatial resolutions (~1 km), (e.g., Balenzano et al., 2012; Balenzano et al., 2021; Paloscia et al., 2013;

76   Peng et al., 2021; Wagner et al., 2013), and have been generalised to peat soil parameters, (Asmuß et

77   al., 2018; Bechtold et al., 2018; Kim et al., 2017; Millard & Richardson, 2018; Millard et al., 2018;

78   Takada et al., 2009). In recent years, Interferometric Synthetic Aperture Radar (InSAR) has been used

79   to estimate peat surface displacements, (Alshammari et al., 2020; Fiaschi et al., 2019), which are

80   known to be linked to peatland ecohydrological conditions, (Regan et al., 2019). For tropical

81   peatlands, this has led to newly proposed methods for estimating GHG emissions on very large scales

82   from InSAR data, (Hoyt et al., 2020; Zhou, 2013; Zhou et al., 2016).

83   Ostensibly, peatlands are an unusual target for the successful use of InSAR time-series methods to

84   derive surface displacement. Vegetated target areas are prone to strong decorrelation of the radar

85   phase over successive radar acquisitions, (Zebker & Villasenor, 1992). This is especially problematic

86   at shorter radar wavelengths (e.g. X-band or C-band), for which penetration of the vegetation by the

87   radar waves is progressively inhibited. Decorrelation in such areas is linked to transient

88   backscattering conditions in the vegetation and/or to variations in underlying soil properties,

89   especially soil moisture (Nesti et al., 1995). Peatlands such as raised bogs or blanket bogs are

90   characterised by a relatively thin (5-50 cm) active vegetation layer, referred as the acrotelm, which

91   when in good condition is dominated by sphagnum mosses. Such vegetation could present more stable

92   backscattering dynamics than other vegetation types (e.g. grasslands), and thus be a factor in the

93   unusually high coherence at peatlands. On the other hand, coherence at peatlands has been noted to

94   decline during seasonal dry periods as the groundwater table declines (Tampuu et al., 2020). Thus

95   soil moisture could exert a complementary or overriding control on coherence, but links between in-

96   situ soil moisture measurements and InSAR data have been lacking.

97   A further complication is that peatlands can be affected by wildfires. Depending on burn duration and

98   intensity, wildfires can cause significant damage to both the active vegetation and the underlying peat,

99   (Wilkinson et al., 2020). In this case, wildfires can potentially change a peatland's ecohydrological

100   state and its ability to sequester carbon (Kettridge et al., 2012; Reddy et al., 2015). For example,

101   Hooijer et al. (2014) defines different relationships between GHG emissions and peatland surface

102   displacements depending on peat conditions (burnt, drained, etc.). Khakim et al. (2020) also shows

103   an increase in peatland subsidence after severe wildfire on tropical peatlands. Understanding of the

104   impact of wildfire on InSAR results for peatlands is thus important for both application and

105   interpretation, but to date has received little if any attention.

106   In this study, we analyse C-band satellite InSAR products, including coherence maps, temporal

107   evolutions of displacements and SAR intensity from Sentinel-1 IW data for a temperate raised bog

108   where soil moisture was measured in-situ over the same time period. The occurrence of a large fire

109   on the bog in June-July 2019 presents an opportunity also to understand the effects of wildfire and

110   sudden peatland vegetation loss on the InSAR products such as coherence and displacement. We first

111   introduce the studied peatland and present the spatial observations from remote sensing via both

112   multispectral and SAR data. We then analyse the links between in-situ soil moisture data and the

113   InSAR parameters, as well as their variations due to the fire. Our results provide new insights into

114   the level at which radar backscattering occurs in a temperate raised peatland and into the impacts of

115   wildfire on InSAR in such a setting. Furthermore, these results highlight key elements for time-series

116   InSAR computation on peatlands to optimise coherence, which will improve the wider application of

117   this remote sensing method to the study of peatlands.

2. Methods

2.1. Study site

Ballynafagh bog is a temperate raised peatland located in Ireland (Co. Kildare), (see Figure 1). The bog is a Special Area of Conservation (SAC), as defined by the European Union's Habitats Directive (Council Directive 92/43/EEC of 21 May 1922). Regional hydrological data suggest that Ballynafagh Bog SAC receives average precipitation of 785 mm.yr^{-1} (1981-2010), with an estimated evapotranspiration rate of ~ 528 mm.yr^{-1}, leaving an average effective precipitation of 257 mm.yr^{-1}: data from MET Éireann (MET), the Irish meteorological service. With an average elevation of 85 m (a.s.l.), the bog has been geomorphologically classified as a basin bog (Kelly, 1993). It is an Irish midland eastern type raised bog, occurring at the eastern limit of the range of raised bogs in Ireland (Cross, 1990). The area is underlain by muddy Carboniferous limestones, interbedded with calcareous shales. The subsoils are predominantly clay-rich glacial tills.

*Figure 1: Ballynafagh bog. **a)** The study area and its surroundings in a Sentinel-2 L1C False Colour image acquired on 2019-06-27, a few days before the wildfire. Coordinates in meters for UTM zone 29U. The blue triangle and red triangle mark the locations of the Central and Sub-Marginal monitoring stations, respectively. The inset shows the location of the study area in Ireland (from Google Earth images). **b)** Post-fire field image, taken on 2019-07-19, of the area around the Central monitoring station. **c)** A post-fire field image, taken on 2019-07-19, of the Sub-marginal monitoring station.*

131   Nearly half the original bog extent within the SAC has been subject to cutting and harvesting of peat

132   in historical times. The uncut high bog has an area of 70 ha and a cutover area of 90 ha. Large drains

133   were installed across the bog throughout the past century for both manual and mechanical peat

134   extraction. Although peat cutting no longer occurs on this site (ceased approximately 2010), no

135   physical restoration measures have been carried out on site. In addition, a significant proportion of

136   the bog was damaged by fire during the mid-1990's.

137   Field mapping in 2013, following the classification of Kelly and Schouten (2002), sub-divided the

138   bog surface into several ecotopes (Figure 2 a). These are areas of similar vegetation type, ecological

139   condition and microtopography, (Fernandez et al., 2014; Kelly & Schouten, 2002). The ecotopes are

140   named Central, Sub-central, Sub-marginal and Marginal, in order of decreasing prevalence of

141   sphagnum mosses and increasing prevalence of heathers and other bushy vegetation. The sphagnum-

142   dominated Central and Sub-central ecotopes represent areas of Active Raised Bog (Fernandez et al.,

143   2014), i.e. bog that "still supports significant areas of vegetation which are normally peat forming".

144   These ARB areas, with a net accumulation of peat, covers 6.48 ha (9.25 %) of the uncut (high) bog

145   area, while the remaining 63.58 ha (90.75 %) of the high bog area consists of non-peat accumulating

146   ecotopes. A Pinus Contorta plantation occurs in the North-West of the bog, which occupies 10.02 ha

147   (20 %) of the high bog area and forms a semi-open canopy. The Face Bank ecotope corresponds to

148   the edge of the high bog where recent cutting has occurred and is characterised by a sharp surface

149   gradient from the high bog to the adjacent lower-lying area of cut-over peat.
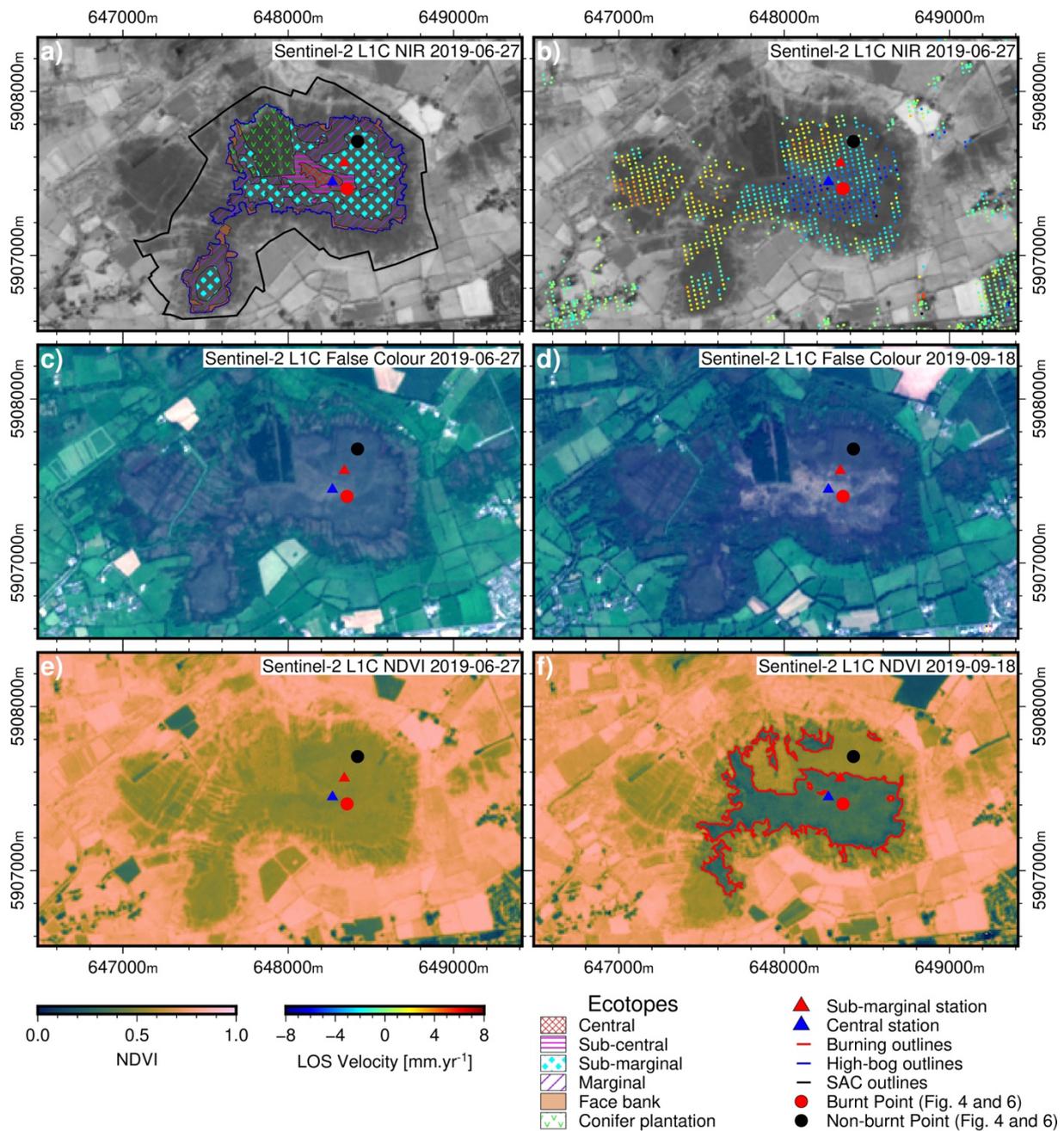
150

Figure 2: Maps of ecotope and remote sensing data for Ballynafagh bog. *a)* Ecotopes of Ballynafagh bog with the NIR Sentinel-2 L1C image on 2019-06-27 as background; *b)* InSAR estimate of peatland surface

*displacements rates in satellite LOS for the period 2017-2021 with NIR Sentinel-2 L1C image on 2019-06-27 as background; **c)-d)** Sentinel-2 L1C false colour images acquired before (on 2019-06-27) and after (on 2019-09-18) the wildfire in July 2019. Spectral bands are Red: 665 nm, Green: 560 nm, Blue: 490 nm; **e)-f)** NDVI from Sentinel-2 L1C images acquired on 2019-06-27 and 2019-09-18 (655 nm and 842 nm), with the outline of burnt areas in red. Coordinates are in meters for UTM zone 29U.*

2.2. In-situ monitoring data

Two soil moisture monitoring stations were installed in the high bog at Ballynafagh in 2017 (Figure 1). The sensors are METER GS3's which measure the dielectric permittivity, and by calibration, the soil moisture of the medium in which the sensor is installed. The sensors were planted at 15 cm depth below the peat surface, following excavation of a shallow hole, which was subsequently back filled using the excavated material. The sensors were installed in Central and Sub-marginal ecotopes on the high bog. They were logged using METER EM50 data loggers from 2017 to 2020, and subsequently using METER ZL6 data loggers. The change in data logger type was made to reduce the possibility of power loss, as occurred on a few occasions in 2018 and 2019. The ZL6 data loggers are solar powered and, since their installation, data has been continuously monitored every 30 minutes. In addition, a piezometer pinned to 1.5 m-depth (with 0.5 m screen) was installed at the Sub-marginal station in March 2019 and functioned with a continuous logging of water table depth until end of October 2020, (sensor: HYDROS 21; logger: METER ZL6).

A post-fire inspection on the 19th of July 2019 revealed that the two monitoring stations had escaped any significant damage by the wildfire. The Central station was located at the southern extremity of a c. 20 m by 10 m "island" of preserved or lightly damaged vegetation (Figure 1 b). The Sub-marginal station was located within the domain of intact vegetation a few metres from the border of main burn

168   area (Figure 1 c). Where impacted, the fire resulted in the removal of almost all surface vegetation on

169   the high bog. It was noted, however, that although the bog surface appeared completely scorched, the

170   fire did not appear to affect the peat below 3-5 cm depth.

171   Time series of daily and hourly precipitation, soil temperature (to 10 cm depth), potential

172   evapotranspiration and evaporation are provided by MET Éireann for the Casement station (Lat.

173   53.303 and Lon. -6.437). This station is twenty kilometres from Ballynafagh bog. Other

174   meteorological stations are closer to the bog, but these record only daily precipitation and atmospheric

175   temperature, whereas Casement station records data hourly and monitors the full range of soil

176   parameters. Since the temperature and precipitation data from Casement station and from the MET

177   stations closest to Ballynafagh bog are very similar (see Supplementary Material), we use the

178   Casement data as a proxy for the local meteorological and soil conditions for the area around

179   Ballynafagh bog.

180   **2.3. SAR data processing**

181   During a SAR acquisition, the satellite emits radar waves that reflect (backscatter) off ground targets

182   and the same satellite measures the return waves. The result is an image containing a complex number

183   in each pixel in radar geometry. The modulus of the complex image (with a normalisation of pixel

184   size - topography) and represents the power of the backscattered signal and is termed the intensity.

185   The argument of the complex image is termed the phase and is related to: (1) the propagation time of

186   the radar waves between the satellite and the ground; (2) the pixel phase, related to the geometry and

187   dielectric properties of the ground targets.

188   The phase information within a single image is not usable because of spatial randomness of the pixel

189   phase, but the difference of phases within two SAR images of the same target area can be calculated

190 to obtain the changes in propagation time. In this case, the phase difference is directly linked to any

191 ground surface displacement that occurred between the two image acquisition dates, as well as to

192 other contributions from topography, satellite orbits, changes in atmospheric conditions, noise, etc.

193 The image obtained by phase differencing is called an interferogram. The stability (i.e. similarity) of

194 the pixel phases between the two SAR acquisitions is termed the coherence (Zebker & Villasenor,

195 1992). Loss of coherence can be called decorrelation.

196 The InSAR method for calculating surface displacements consists of firstly accurately repositioning

197 the one image with respect to the other image (coregistration), and then subtracting or minimising the

198 contributions of all the other sources of phase variation, especially topography and atmosphere

199 (Massonnet & Feigl, 1998). The resultant image is termed a differential interferogram, and hence the

200 method is commonly termed D-InSAR. To obtain the time series of surface displacements - i.e., the

201 evolution of displacements for consecutive SAR acquisitions - an inversion can be done upon a

202 network of differential interferograms. The interferograms can computed either relative to one

203 reference image (single reference network) or relative to several reference dates (multi-reference

204 network) (e.g., Casu et al., 2006; Ferretti et al., 2001). The time elapsed between the acquisitions of

205 the SAR images used to generate each interferogram is termed the temporal baseline. A good network

206 design usually minimises the temporal baselines to maximise coherence (i.e. minimise temporal

207 decorrelation).

208 For this study, InSAR coherence and displacement estimations were derived by processing the

209 Sentinel-1 Single Look Complex (SLC) images acquired in Interferometric Wide Swath mode (IW)

210 in Ascending pass. All available acquisitions between 4th January, 2017 and 18th June 2021 (~4.5

211 years) were used. Images acquired during periods of light snow cover are included in the dataset, but

212 any effects on the results from snow cover are within noise. The coregistration was performed by

213 using the GAMMA® software and the Shuttle Radar Topography Mission (SRTM) Digital Elevation

214 Model (DEM), (Farr et al., 2007; Scheiber & Moreira, 2000; Wegmüller et al., 2015; Wegnüller et

215 al., 2016).

216 From our coregistered SLC stack, the conversion of radar phase to displacement was achieved by

217 using the GAMMA Interferometric Point Target Approach (IPTA) with a multi-reference network of

218 interferograms, which included both single-look and 10/2 multi-look images (kernel-based image

219 averaging to increase signal-to-noise ratio at lower spatial resolution), (Werner et al., 2003). The

220 interferogram network for displacement estimation was created as follows: if N is the index of a SAR

221 acquisition, all N-1, N-2, N-3 interferograms are used together with the N-3 months and N-1 year

222 interferograms, (see Supplementary material). In parallel, coherence maps were computed by using a

223 10 pixels/2 pixels multi-look (same windows as used in IPTA approach) and a 5 pixels/5 pixels

224 estimation kernel (in Radar geometry). Geocoding of images was done with a spatial resolution

225 compatible with the SAR resolution (~ 30 metres). To investigate the variation of coherence around

226 the two in-situ monitoring stations, we used the same estimation parameters, regarding the multi-look

227 kernel and kernel for estimating the coherence, and the coherence was filtered by using a mean kernel

228 of 3 pixels/3 pixels, centred on the pixels containing each station. Thus the coherence around each

229 in-situ stations represents an average value for a ground area of dimension ~ 75 x 125 m.

230 **2.4. Multispectral data processing**

231 To map fire-related vegetation changes at Ballynafagh, we used Sentinel-2 multispectral images at

232 L1C level (without atmospheric correction on radiance measurements) that were acquired before and

233 after the wildfire event. The multispectral bands were cropped and False-Colour, NDVI and IR

234 images were created (band combinations are given in the caption to Figure 2). Without changing the

235 coordinate reference system, the spatial resolution of the optical images is 10 metres. From the post-

236 fire NDVI image, we extract the outlines of burnt areas by using segmentation with a minimum

237 threshold of NDVI = 0.2 and a maximum threshold of NDVI = 0.4. Only burnt areas with an area of

238 at least 25 pixels and non-burnt areas of a minimum of 5 pixels (respecting 4-connected pixels) are

239 selected.

3. Results

3.1. InSAR-derived surface motion velocities

242 Figure 2 b shows the estimated linear velocity of peatland surface motion over the 4.5-year

243 observation period. Each coloured point corresponds to a pixel that displays suitably high coherence

244 and low phase uncertainty throughout the observation period. Overall, point coverage is good across

245 the high bog area, especially in the sphagnum-dominated or sphagnum-rich ecotopes (Central, Sub-

246 central and Sub-marginal). Point retrieval is more challenging in the much of the areas of marginal

247 ecotope, face bank and the cut-over peat. Based on the expected vertical motions for this target, and

248 a conversion factor of 1.3, we can transform the Line of Sight (LOS) displacement to vertical

249 displacements, such that a negative value implies subsidence, and a positive value implies uplift. In

250 general, we consider an absolute velocity of more than 1 mm.yr^{-1} to be significant (Fiaschi et al.,

251 2019).

252 The InSAR velocity data indicate that during the observation period most of the high bog area,

253 straddling the Central, Sub-central, and Sub-marginal ecotopes, has undergone subsidence at average

254 rates of up to -9 mm.yr^{-1}. Several other areas within and just outside the SAC boundary are apparently

255 affected by uplift at average rates of up to +5 mm.yr^{-1}. These areas include a northern part of the high

256 bog classified mainly as Marginal ecotope, as well as zones of cut-over (i.e., harvested) bog to the

257 west. The obtained InSAR-derived velocities are thus dichotomous and somewhat heterogenous, but

258 they overall display a broad consistency in space across the bog.

259 **3.2. RGB and NDVI mapping of the wildfire-affected areas**

260 Sentinel-2 L1C False Colour images with minimal cloud coverage (and similar colour dynamics)

261 show that the burnt areas in the central part of the bog are identifiable by lighter colours in the post-

262 fire image (Figure 2 c-d). By comparing these maps with Figure 1 b-c, we can also see that the Central

263 station is surrounded (preserved on its "island") by burning and that the Sub-marginal station is

264 located at the edge of the burnt area. Furthermore, the NDVI images (c.f., Figure 2 e-f) allow a more

265 precise delimitation of the burnt areas: the NDVI there decreases from a pre-fire value of

266 $0.53 \pm 0.03 (1\sigma)$ to a post-fire value of $0.33 \pm 0.04 (1\sigma)$. In other areas that from field inspection were

267 demonstrably unaffected by the fire, such as the northern part of the high bog (NDVI > 0.5), little or

268 no change in NDVI occurs between the pre-fire and post-fire images. The red contours on Figure 2 d

269 represent the boundaries of areas affect by the fire as derived from the NDVI thresholds. These

270 contours collectively encompass an area of 0.47 km^2, which means that about 60-70 % of the high

271 bog area has been affected and damaged by the wildfire.

272 From other RGB, IR and NDVI images in the Sentinel-2 time series (see Supplementary Materials),

273 we estimate that the wildfire began after 30th June, 2019 and reached its final extent by 7th July, 2019.

274 We are not able to identify the start and end dates of the fire more precisely from the Sentinel-2 data

275 because of cloud cover in many of the multispectral images. Field observations confirm that the

276 wildfire had stopped burning sometime before 19th July, 2019.

3.3. Temporal relations between in-situ soil parameters and InSAR-derived displacements

277

278 The time series of peat surface displacements around the Central and Sub-marginal in-situ monitoring

279 stations (average radius of 25 m) show long-term linear subsidence trends, of $-3.7\pm0.2(1\sigma)$ mm.yr^{-1}

280 and $-1.5\pm0.2(1\sigma)$ mm.yr^{-1}, respectively (Figure 3 a-b). Superimposed on these long-term trends are

281 roughly annual oscillations in surface displacement of up to ±10 mm. Maximum uplift typically

282 occurs between January-March (winter), whereas maximum subsidence typically occurs in June-

283 August (summer).
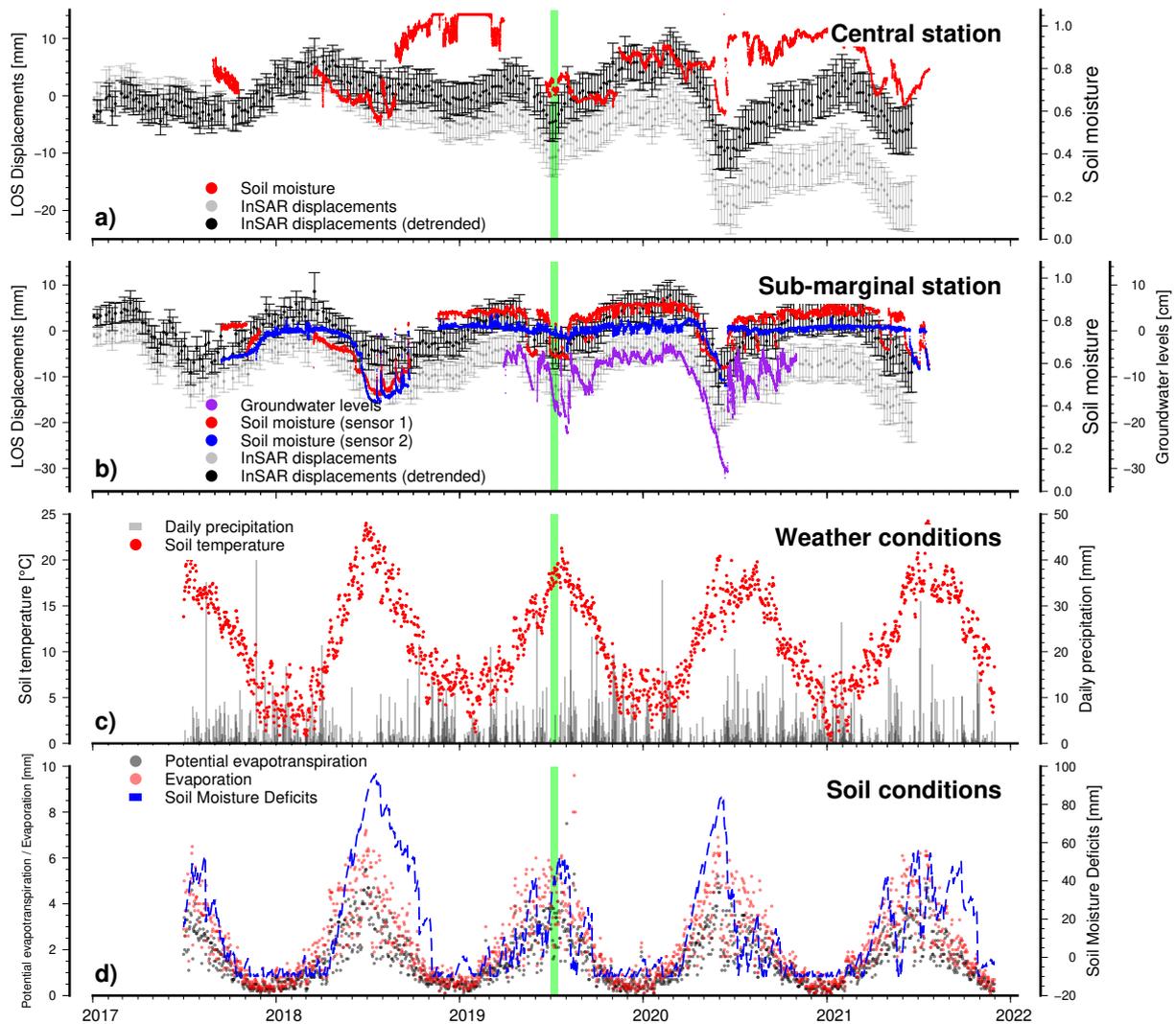
284

Figure 3: Time series of in-situ and remotely-sensed parameters. a)-b) Temporal evolutions of LOS displacements, soil moisture for the Central station (in a)) and the Sub-marginal station (in b)), with the groundwater levels. c) Temporal evolutions of rain precipitation and soil temperature for Casement MET station (Lat. 53.303 and Lon. -6.437) located 22 km from Ballynafagh bog; d) Temporal evolutions of potential evapotranspiration, evaporation, and soil moisture deficits (calculated by using a 'poorly drained' model) for Casement MET station. The estimated duration of the 2019 wildfire event is displayed as a green bar.

285 The temporal evolution InSAR-estimated surface displacement at Ballynafagh bog closely tracks the

286 temporal evolution of soil moisture and groundwater levels measured in-situ (Figure 3 a-b). Soil

287 moisture is highest – typically at saturation (or at sensor detection limit) – during the winter and early

288 spring months. Soil moisture decreases to its lowest values during the summer months. Average

289 groundwater level at the Sub-marginal station is 8 cm below the ground surface, (see Figure 3 b). In

290 winter, the groundwater levels reach up 4 cm below the ground surface, and declines up to 32 cm in

291 summer. Groundwater and soil moisture changes are positively correlated in time. Also the InSAR-

292 derived displacements are near synchronous with both groundwater and soil moisture variations.

293 Although the timescale of seasonal soil moisture and groundwater level decreases is similar to the

294 timescale of seasonal subsidence estimated from InSAR, the recovery of soil moisture and

295 groundwater to high levels is much sharper – i.e. occurs over a much shorter timescale – than the

296 seasonal upswing in surface displacement. Finally, the magnitudes of changes in groundwater and

297 ground surface levels are in ratio of 10:1.

298 The seasonal variations of in-situ soil moisture and InSAR-estimated surface displacement at

299 Ballynafagh bog closely track the meteorological data and soil condition estimates at the regional

300 Casement MET station. The largest amplitudes of surface oscillations at both of the Ballynafagh

301 stations are coincident with periods of low to no rainfall for several weeks (i.e. drought conditions)

302 in Summer 2018 and Summer 2020 (Figure 3 c). These drought periods were characterised by

303 comparably long periods of elevated soil temperatures (Figure 3 c), as well as correspondingly high

304 estimates of evaporation, evapotranspiration and soil moisture deficits (Figure 3 d).

305 The period of the wildfire in 2019 (green bar in Figure 3) is coincident with a period of low soil

306 moisture at Ballynafagh bog (Figure 3 a-b). A sharp decrease in soil moisture (0.8 to 0.7 over 4-5

307 days) can be noted at the Sub-marginal station just before the wildfire. The wildfire occurs also near

308 the summer peak of temperature and a period of rapidly increasing soils moisture deficits as estimated

309 at the regional Casement MET station. It is worth noting that the summer of 2019 was not the warmest

310 or driest in the period from 2017-2021. Ostensibly, conditions may have been more favourable for

311 wildfires in 2018 and 2020, but ignition did not occur.

312 **3.4. Evolution of SAR intensity and InSAR displacement for burned and non-burned areas**

313 Since areas immediately around the monitoring stations seems to have undergone partial burning, we

314 here show data for two areas within the same ecotope (sub-marginal) located further inside the burned

315 and non-burned areas of the peatland. The purpose is to test for contrast in the behaviour of the SAR

316 and InSAR data in the burned and non-burned areas. Data within a 50-m radius of a point in the burnt

317 area (red point in Figure 2) and a point in the non-burnt area (black point in Figure 2) are shown in

318 Figure 4.
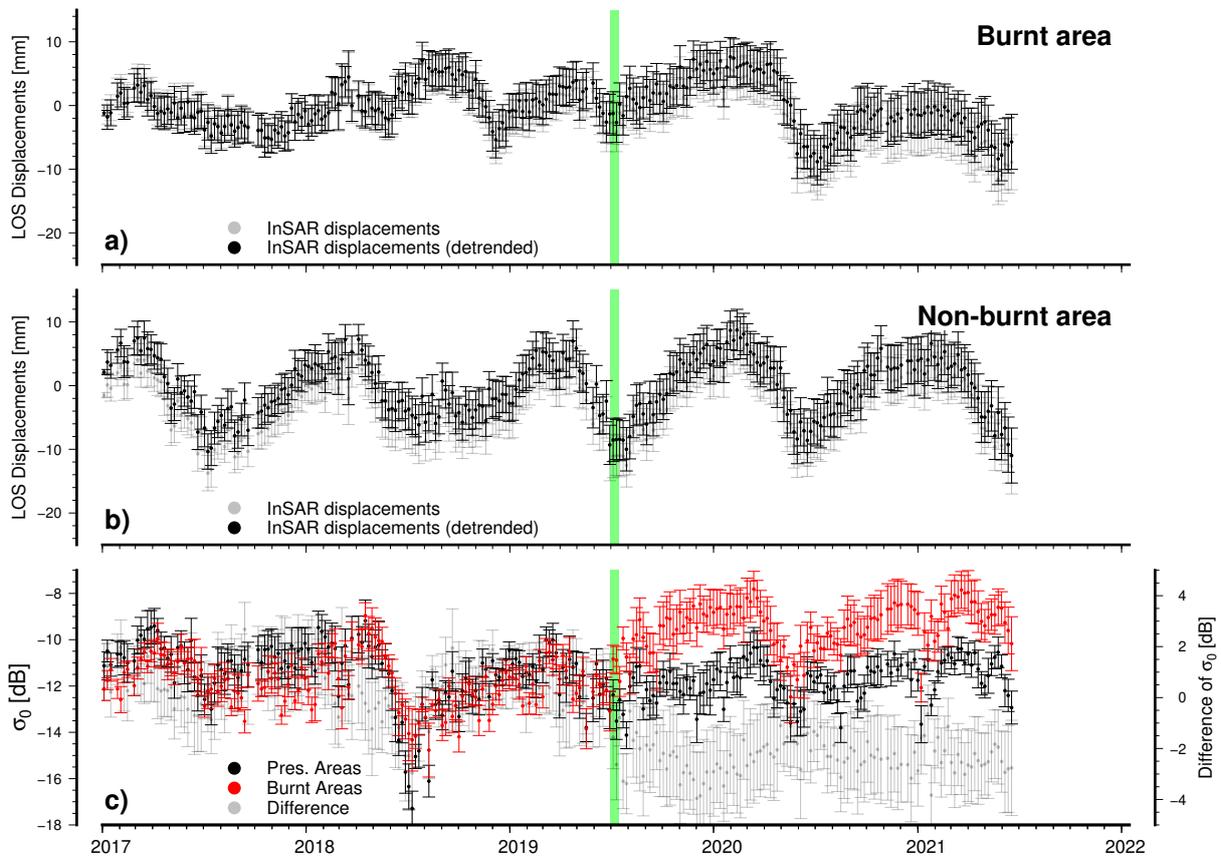
319

*Figure 4: Time series of SAR intensity and displacement for the burnt and non-burnt areas. **a)-b)** Temporal evolutions of LOS displacements for burnt area (in **a)**) and non-burnt area (in **b)**). **c)** Temporal evolution of SAR intensity for burnt and non-burnt areas. The estimated duration of the 2019 wildfire event is displayed as a green bar.*

320 The InSAR displacement time series for both points located show no clear effect due to the wildfire

321 (Figure 4 a-b). The long-term absolute velocities appear to be lower at these points than those

322 observed at the in-situ stations (-0.9±0.2(1σ) mm.yr^{-1} and -0.4±0.2(1σ) mm.yr^{-1} respectively), while

323 the annual oscillations are very similar (Figure 3). The variations in long-term velocity and in the

324 magnitude of annual oscillations further show that the InSAR-derived displacements are dichotomous

325   and heterogenous within the bog. However there is no shift or variation in the burnt area displacement

326   time series that is coincident with the wildfire.

327   On the other hand, the temporal evolutions of the mean SAR backscatter intensity (σ_0) for the burnt

328   and non-burnt areas differ significantly after the wildfire (Figure 4 c). Before the fire, the intensity

329   evolutions of both areas are very similar. After the wildfire period, the relative magnitudes of the

330   annual SAR intensity fluctuations remain equal for both burned and non-burned areas. The SAR

331   intensity of the burnt areas increases overall, however, and it becomes consistently about 2-3 dB

332   higher than that of the preserved areas.

333   **3.5. Evolution of InSAR Coherence**

334   Figure 5 shows the changes in coherence over Ballynafagh bog in the days before and after the

335   wildfire. Overall, the coherence on the bog is high to moderately high for the temporal baselines

336   considered here. There is not a systematic pattern of spatial or temporal change in the coherence that

337   one can relate to the wildfire. The maps with lowest coherence are formed when one SAR image of

338   the pair was acquired on a rainy day – for example, the coherence maps spanning June 23rd - July 5th,

339   June 23rd - July11th, July 23rd - August 4th and July 29th - August 4th. Low coherence thus appears to

340   be simultaneous with differences in precipitation, in groundwater levels, and hence differences in soil

341   moisture, between the pair of SAR image acquisitions. Conversely, high coherence is associated with

342   similar precipitation and soil moisture conditions for the SAR acquisition pair.

343
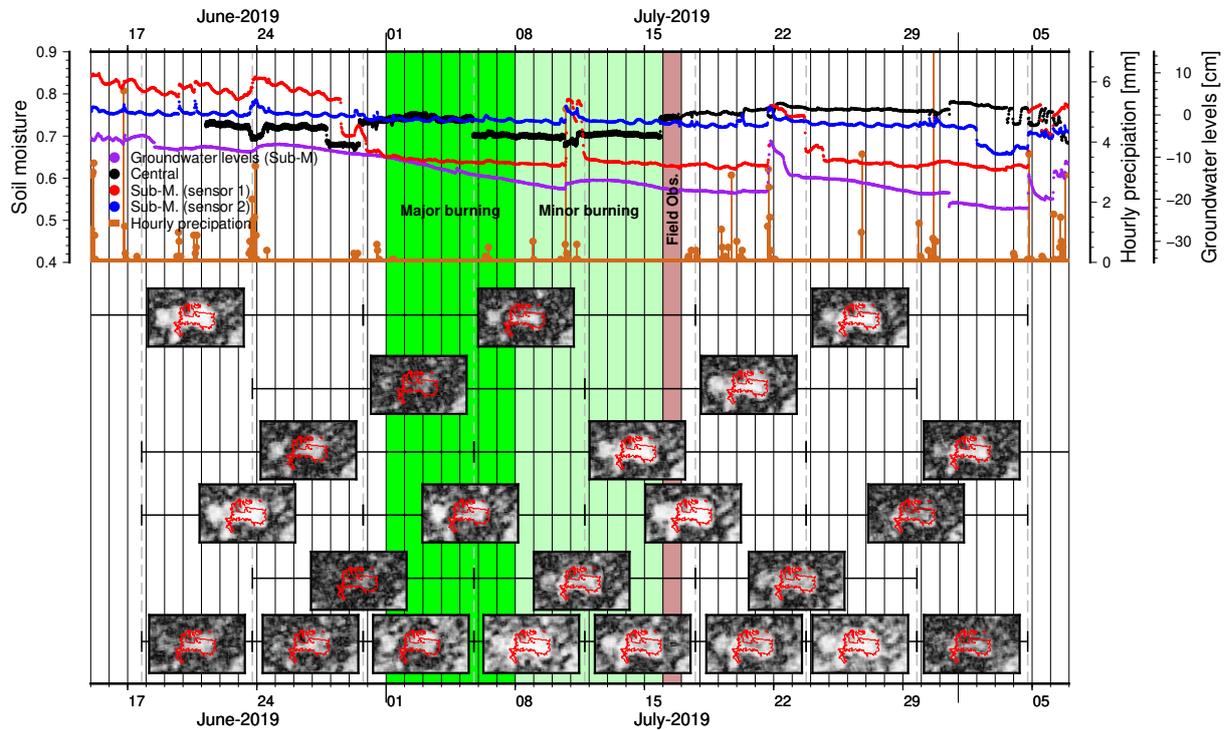
344

Figure 5: Timeline of InSAR coherence maps and soil moisture at Ballynafagh Bog. The upper section shows the temporal evolutions of soil moisture, and groundwater levels as measured at Ballynafagh Bog and hourly precipitation as measured at the Casement MET station. The lower section shows coherence maps for pairs of SAR images, the acquisition dates of which are given by the bars either side of each coherence map. The rows of coherence maps are arranged from top to bottom in order of decreased temporal baseline. In the greyscale coherence maps, black is low coherence and white is high coherence. The red contour is the outline of the areas affected by the wildfire.

345   To illustrate the variation of coherence with soil moisture over the entire observation period, we show

346   a coherence matrix for the areas immediately around both monitoring stations (Figure 6 a). Each point

347   in this matrix represents the coherence in each pair of images in the stack at the Central (upper left)

348   or Sub-marginal (lower right) monitoring stations. The image acquisition dates for the pair are given

349   on the horizontal and vertical axes. We make three main observations from the matrix.

350
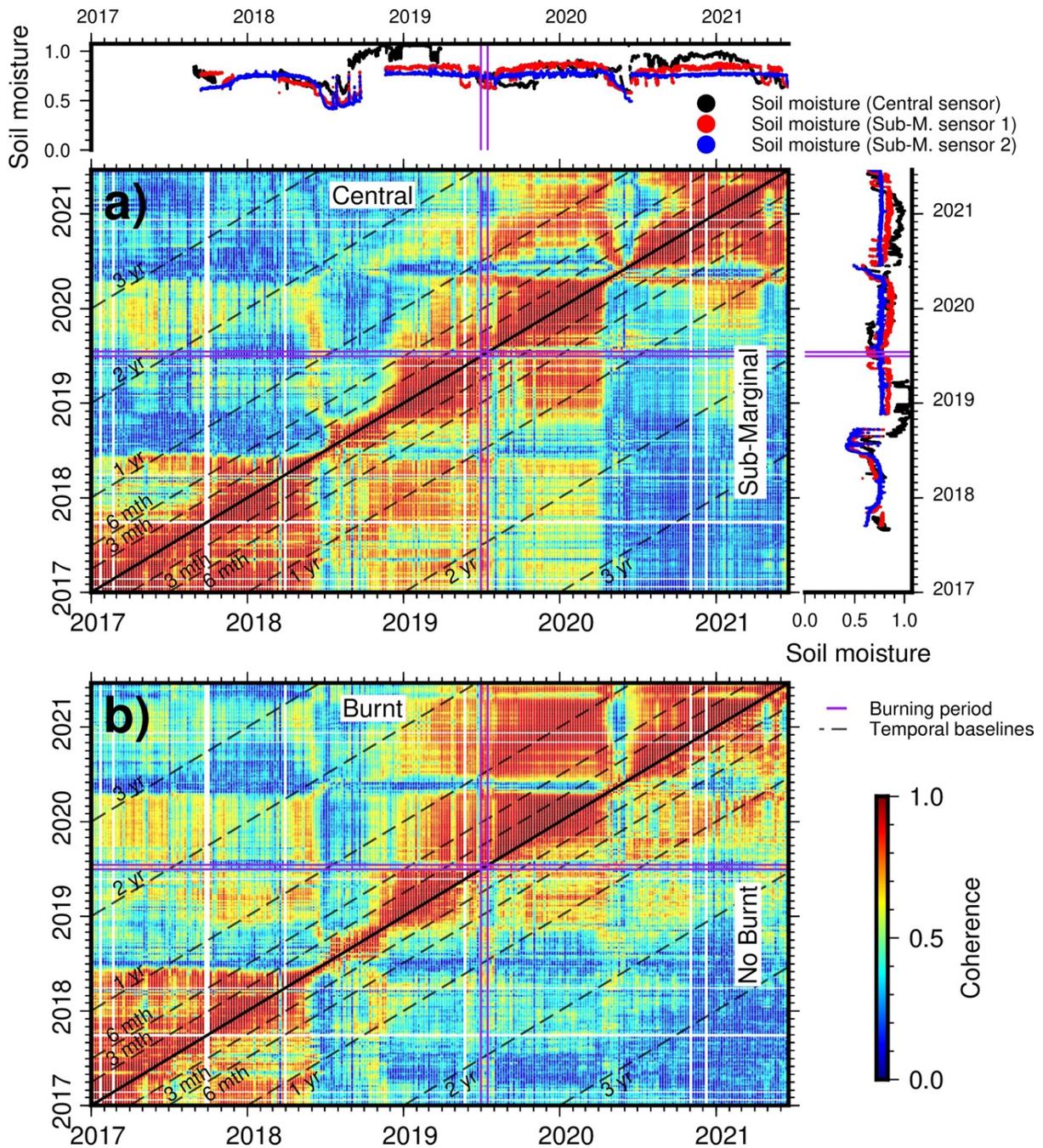
351

*Figure 6: Matrix of coherence for all possible SAR image pairs during the observation period **a)** for the in-situ monitoring stations in Ballynafagh bog and **b)** for the burnt and non-burnt areas as described in Figure 4. For the part **a)**, the upper left triangle of the matrix represents coherence values for the area immediately*

*around the station in the Central ecotope. The lower right triangle, on the other side of the solid black diagonal line, represents values for the area around the station in the Sub-marginal ecotope. For the part **b)**, there is a similar layout for the burnt and the non-burnt areas. The matrix plot axes give the acquisition dates of the two SAR images in each pair. The dashed black lines are isochrons that represent where the temporal baselines of image pairs. For comparison to the temporal evolution of the coherence, the temporal evolution of in-situ soil moisture at both stations is displayed on the plots alongside the matrix in part **a)**. The purple lines crossing the matrix and the plots mark the start and end of the wildfire. Overall, as expected, coherence decreases with increased temporal baseline. For a given temporal baseline, however, coherence is higher when soil moisture conditions are similar for each acquisition in an image pair, and coherence is lower when soil moisture conditions differ substantially.*

352 Firstly, coherence decreases as the temporal baseline of the image pair increases. This is a
353 consequence of temporal decorrelation and is typical of vegetated target areas. This is the main factor
354 controlling coherence on the long term. Secondly, there are abrupt decreases in coherence associated
355 with large differences in soil moisture. These soil moisture-related coherence decreases are
356 superimposed on the background trend of decreased coherence with increased temporal baseline.
357 Coherence loss due to soil moisture difference is particularly pronounced where one SAR image in a
358 pair was acquired during the summers of 2018 or 2020, when large decreases and fluctuations of soil
359 moisture occurred during drought conditions. Under these drought conditions, high coherence (>0.7)
360 interferograms are formed only from image pairs with a temporal baseline of less than 2-3 weeks.
361 Thirdly and from Figure 6 b, the wildfire does not cause a noticeable instantaneous and short-term
362 perturbation on the observed values of coherence compared to the overriding effects of temporal
363 decorrelation and soil moisture difference. The post-burning coherence of the burnt area seems to

364 become slightly higher for longer temporal baselines (>1 year) compared to that of the non-burnt

365 area, but it is unclear if this is a significant change.

4. Discussion

4.1. Link between displacements and peat soil parameters

368 Estimated surface displacements, backscatter intensity and in-situ soil moisture at the raised peatland

369 of Ballynafagh all follow similar temporal fluctuations, with an annual periodicity resulting from dry

370 (spring-summer) and wet (autumn-winter) periods. On the raised bogs, in the absence of human

371 interference, the peat-condition is controlled mainly by short-term seasonal and long-term climatic

372 variation (temperature, rainfall and insolation), which control evapotranspiration and water table

373 levels (Heikurainen et al., 1964). Then, groundwater levels are the driving force of soil moisture. In

374 this case, soil moisture can be a proxy of water-table levels and vice versa, (see Figure 3 b).

375 The long-term displacement trends of subsidence at Ballynafagh bog could be related to internal peat

376 processes, such as peat compaction and oxidation, and potentially to long-term variations in deeper

377 hydrogeological conditions within or under the peatland, (Ewing & Vepraskas, 2006; Regan et al.,

378 2019). It is this long-term part of the displacements that Hooijer et al. (2010), and later Hoyt et al.

379 (2020), propose to use to estimate GHG emissions from InSAR motions on tropical peatlands, (Zhou,

380 2013; Zhou et al., 2016).

381 The short-term (i.e., annual) oscillations in displacement are consistent with annual variations of

382 surface elevation that are commonly measured in-situ on raised peatlands elsewhere. These short-

383 term variations of the peatland surface elevation are termed bog or mire 'breathing', and they are

384   controlled by annual rise and fall in groundwater levels (Fritz et al., 2008; Howie & Hebda, 2018;

385   Zhou et al., 2010). As such, variations in soil moisture and estimated displacements at Ballynafagh

386   bog are likely to be an expression of short-term (annual) water-table changes.

387   Backscatter intensity also shows a seasonal variation that closely mimics that of the estimated surface

388   displacement (Figure 4). The simplest interpretation of this relationship is that backscatter intensity

389   is reduced as the water table falls and soil moisture is reduced - especially in the drought periods.

390   This interpretation is supported by previous work demonstrating a strong positive correlation between

391   backscatter intensity and soil moisture (Dobson et al., 1992). However, the more gradual recovery of

392   both displacement and backscatter intensity compared to the sharper recovery of soil moisture suggest

393   that the radar response is governed not only by soil moisture in the upper unsaturated domain of the

394   peat. The slow recovery of intensity and displacement can be attributed to a slow recovery of the

395   groundwater level after the drought periods. Groundwater levels in the active area of healthy raised

396   bogs such as Ballynafagh typically lie at about 8 cm below the ground surface. As demonstrated here,

397   however, they can drop to several 10s of cm below the surface during drought periods. The backscatter

398   from the peat thus seems to be controlled not only by moisture content in the unsaturated uppermost

399   peat but also by the total saturated volume of the upper 10-30 cm of the organic soil. Future work

400   with co-located piezometers and soil moisture sensors at variable depths in the peat could test this

401   hypothesis.

402   **4.2. Implications of soil moisture changes for InSAR computations**

403   An important observation in our study is that the coherence on a raised peatland can increase over

404   time. This compensates for typical temporal decorrelation on longer temporal baselines (> 1-2 years,

405   and, to our knowledge, this is only observable on peat targets for these durations). The coherence

406 oscillates with the annual frequency with respect to the first coherence value. Indeed, the coherence

407 remains high several months after the master acquisition (about 3 months), decreases for durations of

408 about 6 months, then increases 1 year after the first acquisition, and so on (Figure 6). Thus, it is

409 possible to observe medium or high coherence for 1- or even 2-years temporal baselines.

410 We can easily define that, (after simplifications), (Zhang et al., 2008):

$$\gamma_{Observed} = \gamma_{Temporal} \times \gamma_{Soil\ Moisture} \times \gamma_{Noise} \,, \tag{1}$$

411 with γ the InSAR coherence. With a coherence of 0.7 on the 1-2-years interferograms and equation

412 1, we can interpret that $\gamma_{Temporal}$ is also higher than 0.7, which demonstrates that temporal

413 decorrelation is extremely low on peatlands: probably the lowest compared to other vegetation targets,

414 (Tampuu et al., 2020). In our study case, we show that soil-moisture-related coherence ($\gamma_{Soil\ Moisture}$)

415 is the main factor controlling the recovery of coherence on interferograms with long temporal

416 baselines (>1-2 years), (cf. Figure 6).

417 Conventional and improved InSAR approaches, suitable for peatland applications, are based on

418 interferogram networks selected to minimise temporal and perpendicular baselines, and hence the

419 coherence of the interferogram stack, (e.g., Alshammari et al., 2020; Alshammari et al., 2018; Bateson

420 et al., 2015; Casu et al., 2006; Cigna, Novellino, et al., 2014; Cigna, Sowter, et al., 2014; Hooper,

421 2008; Sowter et al., 2013; Werner et al., 2003). Figure 7 shows the probability of having a coherence

422 higher than 0.5 with respect to the temporal baselines, for each season when the first acquisition

423 (master acquisition) is acquired and for the Sub-marginal station. Due to the temporal evolution of

424 the soil moisture, we can observe that each season offers different evolutions of the probabilities, with

425 two end-members for the winter and summer seasons. In winter and due to the link between the

426 coherence and the soil moisture change, the probability oscillates are caused by the high stability of

427   the soil moisture with the master date. On the contrary, when soil moisture changes for a short period

428   in summer, the probability of having a high coherence is lower, and more controlled by temporal

429   decorrelation. This is particularly true for interferograms with 6-month temporal baselines for which

430   the probability of having an incoherent interferogram is very high. Thus, the coherence is related to

431   the selection of the master date on peatlands: i.e., it seems more robust to select a master acquisition

432   (or super single master regarding the InSAR correlation) in spring in order to maximise the coherence

433   of the whole stack.
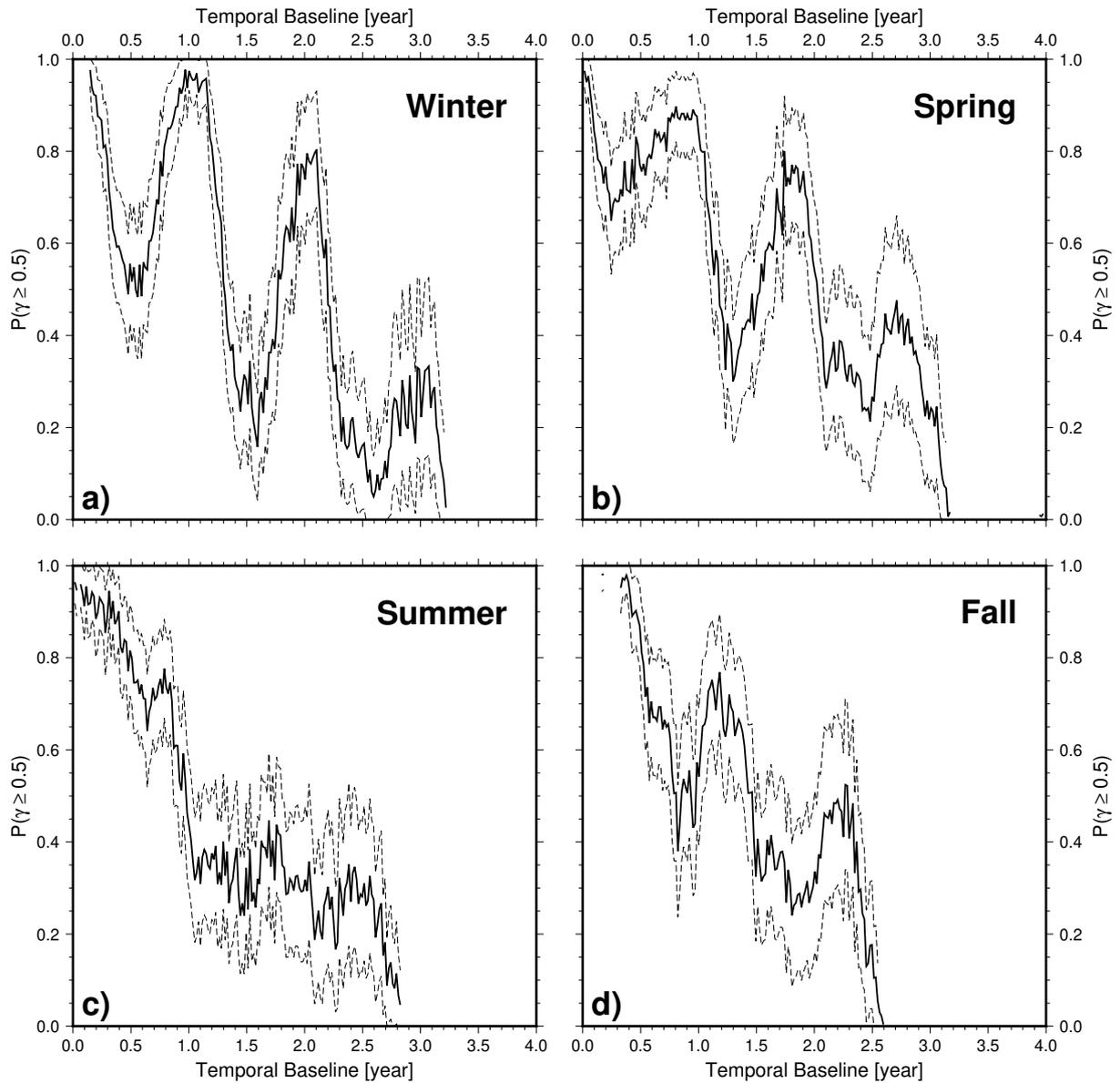
Figure 7: Relations between the probability to have a coherence superior to 0.5 at the Sub-marginal station as a function of temporal baseline, and the season of master acquisition. The dashed lines correspond to 95% confidence levels. The probabilities are estimated using empirical cumulative distribution function (ecdf):
$$P(\gamma \geq 0.5) = 1 - ecdf(0.5).$$

435 According to the proposed InSAR phase and coherence models, the InSAR phase should also be

436 modified by soil moisture (e.g., De Zan et al., 2014). However, we are not able to extract this phase

437 due to the peat surface displacements. In addition, we do not observe significative non-zero closure

438 phases in our interferograms for which we have identified changes in soil moisture. This seems

439 expected because the observation of closure phases is defined by our ability to multi-look and filter

440 the SAR/InSAR data, (Eshqi Molan & Lu, 2020b; Molan et al., 2020). In contrast, high residuals of

441 phase are observed during the InSAR processing. These phase residuals map perfectly to the spatial

442 extent of the bog, and they are unrelated to potential atmospheric delay. The InSAR phase in C band

443 that is interpreted as displacement could therefore include part of unobserved soil moisture phase on

444 the peat targets. This could modify the results during the inversion of displacements and cause an

445 underestimation of the amplitudes of the annual oscillations (in the case of peatlands), (Zwieback et

446 al., 2017). Consequently, InSAR-derived displacement should in future be compared with ground-

447 based displacement measurements to estimate artefacts due to soil moisture on InSAR-derived

448 displacements.

449 **4.3. Interpretation of SAR/InSAR products related to soil moisture changes on raised peatland**

450 The relationships between changes in soil moisture (and vegetation) and SAR/InSAR estimates have

451 been well documented since the beginning of the InSAR studies, whether it is SAR intensity, InSAR

452 phase, coherence or closure phase, (e.g., Barrett, 2012; De Zan & Gomba, 2018; De Zan et al., 2014;

453 De Zan et al., 2015; Nesti et al., 1995; Zhang et al., 2008; Zwieback et al., 2015a, 2015b, 2017).

454 However, the wildfire affecting Ballynafagh bog provides an opportunity to further identify the

455 physical meaning of the SAR/InSAR estimates.

456 Our results for Ballynafagh bog demonstrate that SAR backscatter intensity should be carefully

457 interpreted if used as a proxy for soil moisture where wildfires occur, such as on peatlands. Broadly,

458 SAR intensity is correlated positively with soil moisture at Ballynafagh as expected, (Dobson et al.,

459   1992). The average increase of SAR intensity observed after the wildfire, however, is clearly related

460   to the removal of the mossy vegetation layer by wildfire. The SAR intensity increases in the burnt

461   areas corresponds to the NDVI reduction there (Figure 2 e-f), which we attribute to fire-related

462   vegetation removal (Figure 1 b-c). In support of this interpretation, we note that outside the SAC area

463   containing the bog, similar reductions of NDVI can be seen also in fields within which grass or cereal

464   crops were recently harvested (Figure 2 e-f). Intensity changes are therefore an integration of two

465   layers on the peatlands (mossy and upper peat layers). Without accounting for effects of wildfire,

466   SAR intensity potentially yields overestimations of soil moisture.

467   InSAR coherence has recently emerged as an alternative means of estimating soil moisture, (De Zan

468   & Gomba, 2018; Zwieback et al., 2015b). The aim of InSAR coherence investigations are twofold:

469   (1) to estimate soil moisture at a finer spatial resolution and (2) to correct InSAR-derived

470   displacements, as proposed by Zwieback et al. (2017). However, estimating soil moisture from InSAR

471   coherence and phase appears to be complex and statically unsustainable on conventional soils, (Eshqi

472   Molan & Lu, 2020a). Our InSAR application on a peatland shows a good relationship between peat

473   parameters and the InSAR parameters, which means that InSAR coherence could be an appropriate

474   tool for organic soil moisture estimation in the case of relatively healthy raised peatlands. Moreover,

475   our results demonstrate that InSAR coherence is not affected by changes to vegetation wrought by

476   the early-July 2019 wildfire unlike SAR intensity, InSAR coherence could be more robust to estimate

477   soil moisture on peatlands affected by wildfire.

4.4. Penetration of C-band radar beam into temperate raised peatland

479   The lack of effect of the 2019 wildfire on the InSAR coherence and displacement at Ballynafagh can

480   be interpreted as evidence that the satellite-derived C-band radar waves penetrate into the upper

481   several cm of the peat (Nolan & Fatland, 2003). From Figure 8 which shows a schematic

482   interpretation, the propagation of radar beams is shown for the "pre-fire" and "post-fire" periods.

483   Before the fire, the radar beam firstly penetrates thought the 10-20 cm thick mossy vegetation,

484   attenuating backscatter intensity (approx. -3 to -2 dB). Then the radar waves continue to propagate

485   into the upper few 10's of cm of the underlying peat, where the intensity further decreases and the

486   radar phase (i.e., InSAR phase and coherence) is affected by changes in soil moisture. After the fire

487   and without the 10-20 cm mossy vegetation layer, the intensity increases on average as the vegetation-

488   related attenuation is reduced, but it varies in a positive relationship with the variation of soil moisture

489   in the peat layer.
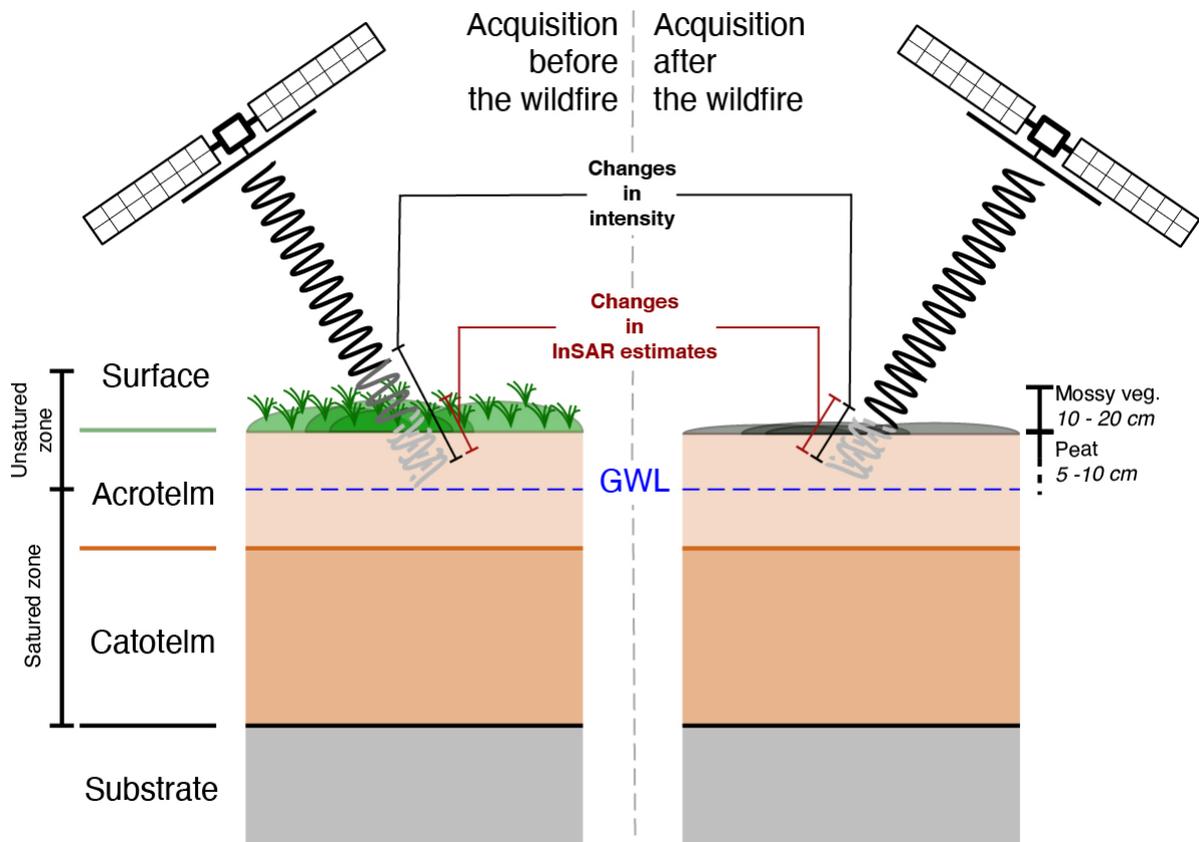
Figure 8: Schematic representation of InSAR propagation in peat associated with climatic controls on soil moisture changes, for active raised bog or healthy areas of bog.

491   In contrast. the InSAR phase and coherence are unaffected by the removal of the vegetation, although

492   they also vary with soil moisture variation. In this case, we interpret that there is a decoupling of the

493   SAR and InSAR measurements on the peatlands. This is because the intensity changes relate to the

494   changes in both soil moisture and vegetation, whereas the InSAR estimates (phase) are not affected

495   by the mossy layer. Therefore, the vegetation layer contributes negligibly to the medium (level)

496   controlling the backscattered radar phase in this raised peatland. Consequently, the SAR and InSAR

497   parameters represent the layers of the peatland.

5. Conclusions

In summary, our study explored the full range of InSAR products and their relationships to in-situ soil moisture and groundwater level measurements over a temperate peatland affected by a wildfire. We draw four main conclusions.

Firstly, the InSAR-estimated peat surface displacements display annual oscillations ("bog breathing") that are synchronous and positively correlated with the seasonal (dry/wet) evolutions of soil moisture and groundwater levels. Thus, peat surface displacements should be an indicator of short-term variations in ecohydrological parameters, such as groundwater levels.

Secondly, SAR intensity positively correlates with absolute values of soil moisture. Thus, SAR intensity oscillates on seasonal timeframes: it increases in wet periods and decreases in dry periods.

Thirdly, InSAR coherence negatively correlates with changes in soil moisture. Consequently, InSAR coherence is low for large soil moisture changes, and is high for small soil moisture changes between two SAR acquisitions. Moreover, the designing of InSAR stack should take into account the relationship to optimise the coherence of the InSAR stack, and avoid coherence loss due to sharp soil moisture changes especially across dry periods.

Fourth, the wildfire highlighted how SAR and InSAR estimates relate to different attributes for raised peatlands: (1) SAR intensity is affected by both changes in soil moisture and vegetation; (2) InSAR coherence is affected by only soil moisture changes. Consequently, SAR and InSAR data from C-band radar sensor reveal information on different levels in the peat column.

These findings can underpin the application and interpretation of radar in monitoring of peatland soil parameters in general and in areas affected by wildfires. Future work should therefore focus on ground

519 validation of InSAR displacements from in-situ measurements in order to verify the accuracy of

520 InSAR results and to identify the possible magnitude of bias caused by soil moisture on displacement

521 observations.

Data availability

523 The additional figures can be found in the Supplementary Materials. All the InSAR products and

524 scripts used to analyse the observations are available from the corresponding authors.

CRediT authorship contribution statement

526 **Alexis Hrysiewicz:** Conceptualisation, Data computation, Investigation and Analysis, Methodology,

527 Visualisation, Writing – original draft. **Eoghan P. Holohan:** Project Funding and administration,

528 Conceptualisation, Investigation and Analysis, Methodology, Visualisation, Writing – original draft,

529 Supervision. **Shane Donohue:** Conceptualisation, in-situ data extraction, Investigation and Analysis.

530 **Hugh Cashnan:** In-situ data extraction and Investigation.

Acknowledgments

Declaration of Competing Interest

The authors declare no competing interests.

References

Alshammari, L., Boyd, D. S., Sowter, A., Marshall, C., Andersen, R., Gilbert, P., Marsh, S., & Large, D. J. (2020). Use of Surface Motion Characteristics Determined by InSAR to Assess Peatland Condition. *Journal of Geophysical Research: Biogeosciences*, *125*(1), 1-15. https://doi.org/10.1029/2018JG004953

Alshammari, L., Large, D. J., Boyd, D. S., Sowter, A., Anderson, R., Andersen, R., & Marsh, S. (2018). Long-term peatland condition assessment via surface motion monitoring using the ISBAS DInSAR technique over the Flow Country, Scotland. *Remote Sensing*, *10*(7). https://doi.org/10.3390/rs10071103

Asmuß, T., Bechtold, M., & Tiemeyer, B. (2018). *Towards Monitoring Groundwater Table Depth in Peatlands from Sentinel-1 Radar Data* IGARSS 2018 - 2018 IEEE International Geoscience and Remote Sensing Symposium, Valencia, Spain.

Balenzano, Mattia, F., Satalino, Pauwels, & Snoeij. (2012). SMOSAR ALGORITHM FOR SOIL MOISTURE RETRIEVAL USING SENTINEL-1 DATA (1) Consiglio Nazionale delle Ricerche (CNR) – Istituto di Studi sui Sistemi Intelligenti per l ' Automazione (ISSIA), Bari , Italy (2) Ghent University – Laboratory of Hydrology a. (1), 1200-1203.

Balenzano, A., Mattia, F., Satalino, G., Lovergine, F. P., Palmisano, D., Peng, J., Marzahn, P., Wegmüller, U., Cartus, O., Dąbrowska-Zielińska, K., Musial, J. P., Davidson, M. W. J., Pauwels, V. R. N., Cosh, M. H., McNairn, H., Johnson, J. T., Walker, J. P., Yueh, S. H., Entekhabi, D., . . . Jackson, T. J. (2021). Sentinel-1 soil moisture at 1 km resolution: a validation study. *Remote Sensing of Environment*, *263*. https://doi.org/10.1016/j.rse.2021.112554

Barrett, B. (2012). The Use of C- and L-Band Repeat-Pass Interferometric SAR Coherence for Soil Moisture Change Detection in Vegetated Areas. *The Open Remote Sensing Journal*, *5*(1), 37-53. https://doi.org/10.2174/1875413901205010037

Bateson, L., Cigna, F., Boon, D., & Sowter, A. (2015). The application of the intermittent SBAS (ISBAS) InSAR method to the South Wales Coalfield, UK. *International Journal of Applied Earth Observation and Geoinformation*, *34*(1), 249-257. https://doi.org/10.1016/j.jag.2014.08.018

Bechtold, M., Schlaffer, S., Tiemeyer, B., & De Lannoy, G. (2018). Inferring Water Table Depth Dynamics from ENVISAT-ASAR C-Band Backscatter over a Range of Peatlands from Deeply-Drained to Natural Conditions. *Remote Sensing*, *10*(4). https://doi.org/10.3390/rs10040536

Casu, F., Manzo, M., & Lanari, R. (2006). A quantitative assessment of the SBAS algorithm performance for surface deformation retrieval from DInSAR data. *Remote Sensing of Environment*, *102*(3-4), 195-210. https://doi.org/10.1016/j.rse.2006.01.023

575 Cigna, F., Novellino, A., Jordan, C. J., Sowter, A., Ramondini, M., & Calcaterra, D. (2014).
576   Intermittent SBAS (ISBAS) InSAR with COSMO-SkyMed X-band high resolution SAR data
577   for landslide inventory mapping in Piana degli Albanesi (Italy). *SAR Image Analysis,*
578   *Modeling, and Techniques XIV*, *9243*, 92431B-92431B. https://doi.org/10.1117/12.2067424
579 Cigna, F., Sowter, A., Jordan, C. J., & Rawlins, B. G. (2014). Intermittent Small Baseline Subset
580   (ISBAS) monitoring of land covers unfavourable for conventional C-band InSAR: proof-of-
581   concept for peatland environments in North Wales, UK. *SAR Image Analysis, Modeling, and*
582   *Techniques XIV*, *9243*, 924305-924305. https://doi.org/10.1117/12.2067604
583 Connolly, J., & Holden, N. M. (2009). Mapping peat soils in Ireland: Updating the derived Irish peat
584   map. *Irish Geography*, *42*(3), 343-352. https://doi.org/10.1080/00750770903407989
585 Connolly, J., Holden, N. M., & Ward, S. M. (2007). Mapping Peatlands in Ireland using a Rule-Based
586   Methodology and Digital Data. *Soil Science Society of America Journal*, *71*(2), 492-499.
587   https://doi.org/10.2136/sssaj2006.0033
588 Cross, J. (1990). *The raised bogs of Ireland: their ecology, status and conservation*. Stationery Office.
589 De Zan, F., & Gomba, G. (2018). Vegetation and soil moisture inversion from SAR closure phases:
590   First experiments and results. *Remote Sensing of Environment*, *217*(2017), 562-572.
591   https://doi.org/10.1016/j.rse.2018.08.034
592 De Zan, F., Parizzi, A., Prats-Iraola, P., & López-Dekker, P. (2014). A SAR interferometric model for
593   soil moisture. *IEEE Transactions on Geoscience and Remote Sensing*, *52*(1), 418-425.
594   https://doi.org/10.1109/TGRS.2013.2241069
595 De Zan, F., Zonno, M., & Lopez-Dekker, P. (2015). Phase Inconsistencies and Multiple Scattering in
596   SAR Interferometry. *IEEE Transactions on Geoscience and Remote Sensing*, *53*(12), 6608-
597   6616. https://doi.org/10.1109/TGRS.2015.2444431
598 Dobson, M. C., Pierce, L., Sarabandi, K., Ulaby, F. T., & Sharik, T. (1992). Preliminary analysis of
599   ERS-1 SAR for forest ecosystem studies. *IEEE Transactions on Geoscience and Remote*
600   *Sensing*, *30*(2), 203-211.
601 Drösler, M., Freibauer, A., Torben, C. R., & Friborg, T. (2008). Observations and status of peatland
602   greenhouse gas emissions in Europe. In *The Continental-Scale Greenhouse Gas Balance of*
603   *Europe* (pp. 243--261). Springer. https://doi.org/10.1007/978-0-387-76570-9
604 Eshqi Molan, Y., & Lu, Z. (2020a). Can InSAR Coherence and Closure Phase Be Used to Estimate
605   Soil Moisture Changes? *Remote Sensing*, *12*(9). https://doi.org/10.3390/rs12091511
606 Eshqi Molan, Y., & Lu, Z. (2020b). Modeling InSAR Phase and SAR Intensity Changes Induced by
607   Soil Moisture. *IEEE Transactions on Geoscience and Remote Sensing*, *58*(7), 4967-4975.
608   https://doi.org/10.1109/tgrs.2020.2970841
609 Ewing, J. M., & Vepraskas, M. J. (2006). Estimating primary and secondary subsidence in an organic
610   soil 15, 20, and 30 years after drainage. *Wetlands*, *26*(1), 119-130.
611   https://doi.org/10.1672/0277-5212(2006)26[119:EPASSI]2.0.CO;2
612 Farr, T. G., Rosen, P. A., Caro, E., Crippen, R., Duren, R., Hensley, S., Kobrick, M., Paller, M.,
613   Rodriguez, E., Roth, L., Seal, D., Shaffer, S., Shimada, J., Umland, J., Werner, M., Oskin, M.,
614   Burbank, D., & Alsdorf, D. E. (2007). The shuttle radar topography mission. *Reviews of*
615   *Geophysics*, *45*(2), RG2004-RG2004. https://doi.org/10.1029/2005RG000183
616 Fernandez, F., Connolly, K., Crowley, W., Deneyer, J., Duff, K., & Smith, G. (2014). *Raised Bog*
617   *Monitoring and Assessment Survey 2013*.
618 Ferretti, A., Prati, C., & Rocca, F. (2001). Permanent scatterers in SAR interferometry. *IEEE*
619   *Transactions on Geoscience and Remote Sensing*, *39*(1), 8-20.
620   https://doi.org/10.1109/36.898661

621 Fiaschi, S., Holohan, E. P., Sheehy, M., & Floris, M. (2019). PS-InSAR Analysis of Sentinel-1 Data
622   for Detecting Ground Motion in Temperate Oceanic Climate Zones: A Case Study in the
623   Republic of Ireland. *Remote Sensing*, *11*(3). https://doi.org/ARTN 348

624 10.3390/rs11030348
625 Fritz, C., Campbell, D. I., & Schipper, L. A. (2008). Oscillating peat surface levels in a restiad
626   peatland, New Zealand-magnitude and spatiotemporal variability. *Hydrological Processes*,
627   *22*(17), 3264-3274. https://doi.org/10.1002/hyp.6912
628 Gorham, E. (1991). Northern Peatlands: Role in the Carbon Cycle and Probable Responses to
629   Climatic Warming. *Ecol Appl*, *1*(2), 182-195. https://doi.org/10.2307/1941811
630 Heikurainen, L., Päivänen, J., & Sarasto, J. (1964). Ground water table and water content in peat soil.
631 Hiraishi, T., Krug, T., Tanabe, K., Srivastava, N., Baasansuren, J., Fukuda, M., & Troxler, T. (2014).
632   2013 supplement to the 2006 IPCC guidelines for national greenhouse gas inventories:
633   Wetlands. *IPCC, Switzerland*.
634 Hooijer, A., Page, S., Canadell, J. G., Silvius, M., Kwadijk, J., Wösten, H., & Jauhiainen, J. (2010).
635   Current and future CO 2 emissions from drained peatlands in Southeast Asia. *Biogeosciences*,
636   *7*(5), 1505-1514. https://doi.org/10.5194/bg-7-1505-2010
637 Hooijer, A., Page, S., Navratil, P., Vernimmen, R., & Mawdsley, N. (2014). Carbon Emissions from
638   Drained and Degraded Peatland in Indonesia and Emission Factors for Measurement ,
639   Reporting and Verification (MRV) of Peatland Greenhouse Gas Emissions. *Forda-*
640   *Mof.Org*(May),   50-50.   http://www.forda-
641   mof.org/files/12._Carbon_Emissions_from_Drained_and_Degraded_Peatland_in_Indonesia.
642   pdf
643 Hooper, A. J. (2008). A multi-temporal InSAR method incorporating both persistent scatterer and
644   small baseline approaches. *Geophysical Research Letters*, *35*(16), L16302-L16302.
645   https://doi.org/10.1029/2008GL034654
646 Howie, S. A., & Hebda, R. J. (2018). Bog surface oscillation (mire breathing): A useful measure in
647   raised   bog   restoration.   *Hydrological   Processes*,   *32*(11),   1518-1530.
648   https://doi.org/10.1002/hyp.11622
649 Hoyt, A. M., Chaussard, E., Seppalainen, S. S., & Harvey, C. F. (2020). Widespread subsidence and
650   carbon emissions across Southeast Asian peatlands. *Nature Geoscience*, *13*(6), 435-440.
651   https://doi.org/10.1038/s41561-020-0575-4
652 Jones , K., Lanthier, Y., van der Voet, P., van Valkengoed, E., Taylor, D., & Fernandez-Prieto, D.
653   (2009). Monitoring and assessment of wetlands using Earth Observation: The GlobWetland
654   project.   *Journal   of   Environmental   Management   90*,   2154-2169.
655   https://doi.org/10.1016/j.jenvman.20 07.07.037
656 Kelly, L. (1993). *Hydrology, Hydrochemistry and Vegetation of Two Raised Bogs in Co. Offaly* Ph.
657   D. Thesis. Trinity College, Dublin. Available at: http://www. npws. ie …].
658 Kelly, L., & Schouten, M. G. C. (2002). Vegetation. In M. G. C. Schouten (Ed.), *Conservation and*
659   *restoration of raised bogs: geological, hydrological and ecological studies* (pp. 110-169). The
660   Heritage Service of the Department of the Environment and Local Government, Ireland;
661   Staatsbosbeheer, the Netherlands; Geological Survey of Ireland, Dublin.
662 Kettridge, N., Thompson, D. K., & Waddington, J. M. (2012). Impact of wildfire on the thermal
663   behavior of northern peatlands: Observations and model simulations. *Journal of Geophysical*
664   *Research: Biogeosciences*, *117*(G2), n/a-n/a. https://doi.org/10.1029/2011jg001910

665 Khakim, M. Y. N., Bama, A. A., Yustian, I., Poerwono, P., Tsuji, T., & Matsuoka, T. (2020). Peatland
666   subsidence and vegetation cover degradation as impacts of the 2015 El niño event revealed
667   by Sentinel-1A SAR data. *International Journal of Applied Earth Observation and*
668   *Geoinformation*, *84*. https://doi.org/10.1016/j.jag.2019.101953
669 Kim, J.-W., Lu, Z., Gutenberg, L., & Zhu, Z. (2017). Characterizing hydrologic changes of the Great
670   Dismal Swamp using SAR/InSAR. *Remote Sensing of Environment*, *198*, 187-202.
671   https://doi.org/10.1016/j.rse.2017.06.009
672 Köchy, M., Hiederer, R., & Freibauer, A. (2015). Global distribution of soil organic carbon – Part 1:
673   Masses and frequency distributions of SOC stocks for the tropics, permafrost regions,
674   wetlands, and the world. *Soil*, *1*(1), 351-365. https://doi.org/10.5194/soil-1-351-2015
675 Lees, K. J., Quaife, T., Artz, R. R. E., Khomik, M., & Clark, J. M. (2018). Potential for using remote
676   sensing to estimate carbon fluxes across northern peatlands – A review. *Science of the Total*
677   *Environment*, *615*, 857-874. https://doi.org/10.1016/j.scitotenv.2017.09.103
678 Leifeld, J., & Menichetti, L. (2018). The underappreciated potential of peatlands in global climate
679   change mitigation strategies /704/47/4113 /704/106/47 article. *Nature Communications*, *9*(1).
680   https://doi.org/10.1038/s41467-018-03406-6
681 Massonnet, D., & Feigl, K. L. (1998). Radar interferometry and its application to changes in the
682   earth's surface. *Reviews of Geophysics*, *36*(4), 441-500. https://doi.org/10.1029/97RG03139
683 Millard, K., & Richardson, M. (2018). Quantifying the relative contributions of vegetation and soil
684   moisture conditions to polarimetric C-Band SAR response in a temperate peatland. *Remote*
685   *Sensing of Environment*, *206*(December 2017), 123-138.
686   https://doi.org/10.1016/j.rse.2017.12.011
687 Millard, K., Thompson, D. K., Parisien, M. A., & Richardson, M. (2018). Soil moisture monitoring
688   in a temperate peatland using multi-sensor remote sensing and linear mixed effects. *Remote*
689   *Sensing*, *10*(6). https://doi.org/10.3390/rs10060903
690 Molan, Y. E., Lu, Z., & Kim, J.-W. (2020). Influence of the Statistical Properties of Phase and
691   Intensity on Closure Phase. *IEEE Transactions on Geoscience and Remote Sensing*, *58*(10),
692   7346-7354. https://doi.org/10.1109/tgrs.2020.2982062
693 Nesti, G., Tarchi, D., & Rudant, J.-P. (1995). Decorrelation of backscattered signal due to soil
694   moisture changes. IEEE International Symposium on Geoscience and Remote Sensing,
695   Firenze, Italy.
696 Nolan, M., & Fatland, D. R. (2003). Penetration depth as a DInSAR observable and proxy for soil
697   moisture. *IEEE Transactions on Geoscience and Remote Sensing*, *41*(3), 532-537.
698   https://doi.org/10.1109/tgrs.2003.809931
699 Paloscia, S., Pettinato, S., Santi, E., Notarnicola, C., Pasolli, L., & Reppucci, A. (2013). Soil moisture
700   mapping using Sentinel-1 images: Algorithm and preliminary validation. *Remote Sensing of*
701   *Environment*, *134*, 234-248. https://doi.org/10.1016/j.rse.2013.02.027
702 Parish, F., Sirin, A., Charman, D., Joosten, H., Minayeva, T., Silvius, M., & Stringer, L. (2008).
703   *Assessment on Peatlands, Biodiversity and Climate Change: Main Report. Global*
704   *Environment Centre, Kuala Lumpur and Wetlands International, Wageningen*.
705 Peng, J., Albergel, C., Balenzano, A., Brocca, L., Cartus, O., Cosh, M. H., Crow, W. T., Dabrowska-
706   Zielinska, K., Dadson, S., Davidson, M. W. J., de Rosnay, P., Dorigo, W., Gruber, A.,
707   Hagemann, S., Hirschi, M., Kerr, Y. H., Lovergine, F., Mahecha, M. D., Marzahn, P., . . . Loew,
708   A. (2021). A roadmap for high-resolution satellite soil moisture applications – confronting
709   product characteristics with user requirements. *Remote Sensing of Environment*, *252*.
710   https://doi.org/10.1016/j.rse.2020.112162

711 Reddy, A. D., Hawbaker, T. J., Wurster, F., Zhu, Z., Ward, S., Newcomb, D., & Murray, R. (2015).
712   Quantifying soil carbon loss and uncertainty from a peatland wildfire using multi-temporal
713   LiDAR. *Remote Sensing of Environment*, *170*, 306-316.
714   https://doi.org/10.1016/j.rse.2015.09.017
715 Regan, S., Flynn, R., Gill, L., Naughton, O., & Johnston, P. (2019). Impacts of Groundwater Drainage
716   on Peatland Subsidence and Its Ecological Implications on an Atlantic Raised Bog. *Water
717   Resources Research*, *55*(7), 6153-6168. https://doi.org/10.1029/2019WR024937
718 Renou-Wilson, F., Moser, G., Fallon, D., Farrell, C. A., Müller, C., & Wilson, D. (2019). Rewetting
719   degraded peatlands for climate and biodiversity benefits: Results from two raised bogs.
720   *Ecological Engineering*, *127*, 547-560. https://doi.org/10.1016/j.ecoleng.2018.02.014
721 Roulet, N. T. (2000). Peatlands, carbon storage, greenhouse gases, and the kyoto protocol: Prospects
722   and significance for Canada. *Wetlands*, *20*(4), 605-615. https://doi.org/10.1672/0277-
723   5212(2000)020[0605:PCSGGA]2.0.CO;2
724 Scheiber, R., & Moreira, A. (2000). Coregistration of interferometric SAR images using spectral
725   diversity. *IEEE Transactions on Geoscience and Remote Sensing*, *38*(5), 2179-2191.
726   https://doi.org/10.1109/36.868876
727 Sowter, A., Bateson, L., Strange, P., Ambrose, K., & Fifiksyafiudin, M. (2013). Dinsar estimation of
728   land motion using intermittent coherence with application to the south derbyshire and
729   leicestershire coalfields. *Remote Sensing Letters*, *4*(10), 979-987.
730   https://doi.org/10.1080/2150704X.2013.823673
731 Takada, M., Mishima, Y., & Natsume, S. (2009). Estimation of surface soil properties in peatland
732   using ALOS/PALSAR. *Landscape and Ecological Engineering*, *5*(1), 45-58.
733   https://doi.org/10.1007/s11355-008-0061-4
734 Tampuu, T., Praks, J., Uiboupin, R., & Kull, A. (2020). Long Term Interferometric Temporal
735   Coherence and DInSAR Phase in Northern Peatlands. *Remote Sensing*, *12*(10).
736   https://doi.org/10.3390/rs12101566
737 Wagner, W., Sabel, D., Doubkova, M., Bartsch, A., & Pathe, C. (2013). the Potential of Sentinel-1 for
738   Monitoring Soil Moisture With a High Spatial Resolution At Global Scale. *Cycle*,
739   *2009*(November 2009), 18-20.
740 Wegmüller, U., Werner, C., Strozzi, T., Wiesmann, A., Frey, O., & Santoro, M. (2015). Sentinel-1
741   IWS mode support in the GAMMA software. 2015 IEEE 5th Asia-Pacific Conference on
742   Synthetic Aperture Radar (APSAR),
743 Wegnüller, U., Werner, C., Strozzi, T., Wiesmann, A., Frey, O., & Santoro, M. (2016). Sentinel-1
744   Support in the GAMMA Software. *Procedia Computer Science*, *100*, 1305-1312.
745   https://doi.org/10.1016/j.procs.2016.09.246
746 Werner, C., Wegmüller, U., Strozzi, T., & Wiesmann, A. (2003). Interferometric point target analysis
747   for deformation mapping. IGARSS 2003. 2003 IEEE International Geoscience and Remote
748   Sensing Symposium.,
749 Wilkinson, S. L., Tekatch, A. M., Markle, C. E., Moore, P. A., & Waddington, J. M. (2020). Shallow
750   peat is most vulnerable to high peat burn severity during wildfire. *Environmental Research
751   Letters*, *15*(10). https://doi.org/10.1088/1748-9326/aba7e8
752 Xu, J., Morris, P. J., Liu, J., & Holden, J. (2018). PEATMAP: Refining estimates of global peatland
753   distribution based on a meta-analysis. *Catena*, *160*, 134-140.
754 Yu, Z., Loisel, J., Brosseau, D. P., Beilman, D. W., & Hunt, S. J. (2010). Global peatland dynamics
755   since the Last Glacial Maximum. *Geophysical Research Letters*, *37*(13), n/a-n/a.
756   https://doi.org/10.1029/2010gl043584

757 Zebker, H. A., & Villasenor, J. (1992). Decorrelation in Interferometric Radar Echoes. *IEEE*
758   *Transactions on Geoscience and Remote Sensing*, *30*(5), 950-959. https://doi.org/Doi
759   10.1109/36.175330
760 Zhang, T., Zeng, Q., Li, Y., & Xiang, Y. (2008). *Study on relation between InSAR coherence and soil*
761   *moisture* XXIst ISPRS Congress Technical Commission VI, Beijing, China.
762 Zhou, Z. (2013). *The applications of InSAR time series analysis for monitoring long-term surface*
763   *change in peatlands*
764 Zhou, Z., Li, Z., Waldron, S., & Tanaka, A. (2016). Monitoring peat subsidence and carbon emission
765   in Indonesia peatlands using InSAR time series. *International Geoscience and Remote*
766   *Sensing   Symposium   (IGARSS)*,   *2016-November*,   6797-6798.
767   https://doi.org/10.1109/IGARSS.2016.7730774
768 Zhou, Z., Waldron, S., & Li, Z. (2010). Integration of PS-InSAR and GPS for monitoring seasonal
769   and long-term peatland surface fluctuations. Remote Sensing and the Carbon Cycle,
770 Zwieback, S., Hensley, S., & Hajnsek, I. (2015a). Assessment of soil moisture effects on L-band radar
771   interferometry.   *Remote   Sensing   of   Environment*,   *164*,   77-89.
772   https://doi.org/10.1016/j.rse.2015.04.012
773 Zwieback, S., Hensley, S., & Hajnsek, I. (2015b). A Polarimetric First-Order Model of Soil Moisture
774   Effects   on   the   DInSAR   Coherence.   *Remote   Sensing*,   *7*(6),   7571-7596.
775   https://doi.org/10.3390/rs70607571
776 Zwieback, S., Hensley, S., & Hajnsek, I. (2017). Soil Moisture Estimation Using Differential Radar
777   Interferometry: Toward Separating Soil Moisture and Displacements. *IEEE Transactions on*
778   *Geoscience   and   Remote   Sensing*,   *55*(9),   5069-5083.
779   https://doi.org/10.1109/tgrs.2017.2702099